Blazar Counterparts for 3EG sources at -40 < decl. < 0: Pushing South through the Bulge

David Sowards-Emmerd[1], Roger W. Romani & Peter F. Michelson[1]

Department of Physics, Stanford University, Stanford, CA 94305

dse@darkmatter.stanford.edu, rwr@astro.stanford.edu, peterm@stanford.edu

James S. Ulvestad

National Radio Astronomy Observatory, Socorro, NM 87801

julvesta@nrao.edu

ABSTRACT

Supplementing existing survey data with VLA observations, we have extended $\gamma-$ray counterpart identifications down to decl. = -40° using our Figure of Merit approach. We find blazar counterparts for $\sim$ 70% of EGRET sources above decl. = -40° away from the Galaxy. Spectroscopic confirmation is in progress, and spectra for $\sim$ two dozen sources are presented here. We find evidence that increased exposure in the bulge region allowed EGRET to detect relatively faint blazars; a clear excess of non-blazar objects in this region however argues for an additional (new) source class.

Subject headings: AGN: blazars – surveys: radio – surveys: optical – Gamma Rays

1. Introduction

The *EGRET* telescope on the Compton Gamma Ray Observatory (CGRO) satellite has detected 271 sources in a survey of the γ-ray (100 MeV to 10 GeV) sky. Roughly one quarter of these have previously been identified as blazars (Hartman *et al.* 1999; Mattox *et al.* 2001). Recently, we have developed a new counterpart identification technique, which has pushed the identified fraction to $\sim$70% in the northern hemisphere (Sowards-Emmerd *et al.* 2003,

[1]also, Stanford Linear Accelerator Center, Stanford, CA, 94039-4349

hereafter SRM03). Here, we extend the application of this technique south (-40° < decl. < 0°), including the Galactic bulge region. In order to rank blazar candidates in this zone using our 'Figure of Merit' (FoM) method, we have selected flat spectrum radio counterpart candidates in 3EG source error boxes. We have obtained spectroscopic confirmations and estimated redshifts for many of these candidate blazars with the Hobby-Eberly Telescope (HET) Marcario Low Resolution Spectrograph (LRS) and with the 2.7-m Harlan J. Smith Telescope IGI spectrograph at McDonald Observatory. For our final counterpart list, we used the VLA to obtain compact 8.4 GHz fluxes similar to those previously mined from the CLASS (Meyers *et al.* 2002) survey. This allows a robust selection of EGRET blazar-like counterparts and a statistical measure of the identification probability of each source.

The blazar label is somewhat heterogeneous, but in the context of the unified AGN model, these sources are believed to be viewed close to the axis of a powerful relativistic jet. As such they are compact flat spectrum radio sources, with apparent superluminal motion at VLBI scales. The optical counterparts exhibit significant polarization and OVV (optically violently variable) behavior (Urry & Padovani 1995). Optical spectroscopy yields a dichotomy of sources: flat spectrum radio quasars with broad emission lines and continuum-dominated BL Lac-type objects showing weak absorption features and occasionally narrow, weak emission lines. The broad-band spectral energy distribution (SED) is sometimes used to divide these into two classes, with 'red' blazars showing a synchrotron peak in the IR-optical with a Synchrotron Self-Compton (SSC) peak in the γ-ray while 'blue' blazars have a synchrotron component extending into the X-ray with a SSC peak inferred to extend to the TeV range (Urry 1999, and references therein).

2. Candidate Selection and Figure of Merit

In our previous analysis (SRM03), we quantified the correlation between flat spectrum radio sources and 3EG positions. This approach produces a quantitative evaluation of the likelihood of each counterpart candidate, based on radio flux, radio spectral index, X-ray flux, and location of the source within a 3EG error box. The independent functions used to generate this 'Figure of Merit' (FoM) statistic took the form of a fractional excess of sources found within the 3EG positional 95% confidence contours, in a given flux or spectral index bin, relative to the random background sources:

$$n = \frac{N_{3EG} - N_{Random}}{N_{3EG}} \tag{1}$$

These functions, combined with the positional likelihood $L(\alpha, \delta)$, form our FoM:

$$FoM = n_{8.4GHz} \times n_{\alpha} \times n_{X-ray} \times L(\alpha, \delta) \tag{2}$$

The details of the FoM analysis are described in SRM03. Here it is worth noting that the adopted fitting functions take the radio FoM to zero at $S_{8.4} = 85$ mJy and the spectral index FoM to zero at α =0.53, where $S_\nu \propto \nu^{-\alpha}$.

To generate a FoM for southern/bulge sources equivalent to those of the Northern sample, accurate, compact 8.4 GHz fluxes were essential. Source selection for 8.4 GHz VLA A-Array observations proceeded in a similar fashion to that for the CLASS survey. We first selected NVSS (1.4 GHz; Condon *et al.* 1998) sources within 90 arcseconds of PMN (4.85 GHz; Gregory *et al.* 1996) single dish source positions, for PMN sources in the TS maps of 3EG catalog sources in the range -40° < decl. < 0°. The 'Test Statistic' TS is the maximum likelihood estimator used in the EGRET source catalogs to quantify the probability that an EGRET point source is at a given location; contours of ΔTS from the maximum define the source uncertainty region. For each 1.4 GHz source a spectral index was computed; if multiple NVSS sources matched one PMN source, the NVSS fluxes were summed and the average 1.4/4.8 GHz spectral index was applied to each. Sources with spectral indices steeper than 0.5, the CLASS spectral index cut, were dropped from consideration. Additionally, a conservative spectral index lower limit of -2.0 was applied. Such strongly inverted spectral indices are consistent with optically thick thermal emission and we expect these sources to be Galactic (planetary nebulae and HII regions). Blazars generally do not exhibit spectra nearly this inverted. The CLASS blazar survey (Marcha *et al.* 2001) contains 6 sources (of 325) with $\alpha_{1.4/4.8} < -0.8$ and only one of these has been optically identified as a blazar. The Deep X-ray Blazar Survey (Perlman *et al.* 1998; Landt *et al.* 2001) find only 2 sources (of 298) with $\alpha_{1.4/4.8} < -0.6$ and none with $\alpha_{1.4/4.8} < -0.8$.

Using these spectral indices, we then computed preliminary 8.4 GHz flux estimates. X-ray fluxes were mined from the ROSAT All-Sky Survey bright and faint catalogs. From the estimated 8.4 GHz flux, the spectral index, the X-ray flux, and the ΔTS at the position of the radio source, the FoM was calculated. Sources located at values of ΔTS > 13.5 were not considered. We have made a conservative cut of FoM > 0.125, half the threshold for inclusion as 'plausible' identifications in SRM03, to allow for errors in the spectral index and the flux extrapolation to 8.4 GHz. Blazars are significantly variable and our radio survey observations are not simultaneous, so it is important to note this is a significant source of error in the spectral index estimates. Source confusion in the large PMN beam and measurement uncertainties for the fainter sources may also contribute. PMN observations were made in 1990, while the NVSS observations spanned 1993-1996. Sources meeting this preliminary FoM > 0.125 criterion were targeted for VLA 8.4 GHz follow-up.

3. VLA Observations

CLASS 8.4 GHz fluxes are in general not available below decl.= 0°. Thus, to establish a spectral index and flux for the sources equivalent to that used in SRM03, sources above the preliminary FoM threshold were observed at 8.4 GHz with the VLA A-array during 23-25 July 2003 (Program AR517). Observations were taken with a bandwidth of 50 MHz in each IF and typically two 2-3 minute scans were taken per source. In practice, a number of targets in the original candidate list were not observed in this campaign. A handful of EGRET error boxes at low latitude contained very large numbers of sources, likely due to extended Galactic emission. These were not observed, although a number of the candidates in these regions formally met our 1.4 GHz/4.85 GHz survey cuts. At higher latitude a few additional sources were missed due to clerical error. In the analysis that follows we use the 1.4/4.85 spectral indices and extrapolated fluxes for these objects. Several of these sources are very likely to be thermal, but a few deserve interferometric follow up and our classification of these should be viewed as preliminary. Archival 8.4 GHz fluxes were mined from the VLA Calibrator database for several of the brightest sources. Several of the target sources were in fact used as VLA phase calibrators during the observation run. A total of 102 sources were observed in this campaign.

The data were edited and calibrated with the NRAO Astronomical Image Processing System (AIPS) package in the usual manner. Maps were created, self-calibrated and cleaned using AIPS. A single-component model was employed in the self-calibration. Self-calibration was not performed on a handful of the faintest (few mJy) sources. Finally, peak intensities of the sources were fit. All of the bright sources were strongly core dominated, although about 20% show jets on 0.1-1 arcsec scales, consistent with the blazar classification. The typical noise level was less than 1 mJy/beam. Except for the faintest sources, the flux errors are dominated by calibration uncertainties at these low declinations (estimated at $\sim$3%). Fluxes of sources that meet our FoM threshold appear in Table 1. Figure 1 shows the images for our highest probability new identifications. Precise positions and core fluxes for all observed sources are in Table 4. The remainder of the images will be provided upon request.

Several sources showed no compact flux, and a handful gave fluxes much lower than expected from our extrapolated values. Indeed all but one of the sources with $\alpha_{1.4-4.8}$ <-0.8 had little compact 8.4 GHz flux. Several of these sources can be identified as extended HII regions and planetary nebulae. Based on this result, we believe that the sources classified as (G) in Table 1 are in fact Galactic. We note that many of these objects have spectral indices consistent with an optically thick thermal spectrum, $\alpha = -2$. However, as Halpern *et al.* (2001) have pointed out, blazars at low latitude can be masked in the radio by Galactic objects, as in the case of 3EG J2016+3657. To be conservative, we denote these as

unclassified sources in our summary Aitoff plot.

It should be noted that 1.4-8.4 GHz spectral indices are generally steeper than 1.4-4.8 GHz spectral indices based on the PMN fluxes. This is also seen in the CLASS blazar survey (Marcha *et al.* 2001).

4. Optical Follow-up

The majority of our radio selected blazar candidates have archival optical classifications and redshifts. Information for these objects were extracted from the SIMBAD and NED databases. We have targeted the remainder of the sources for spectroscopic followup at McDonald Observatory.

Spectroscopy was obtained using the Marcario LRS (Hill et al. 1998) on the 9.2 m HET (Ramsey et al. 1998). These targets were observed in regular queue operations between April 2003 and July 2003. We obtained 2 × 300s exposures for most targets, and 3 × 300s for fainter targets. Observations were made employing a 300 line mm^{-1} grating and a $2''$ slit, giving a dispersion of 4Å per (binned) pixel and an effective resolution of 16Å covering $\lambda\lambda 4200 - 10000$Å.

Due to the pointing limitations of the HET (decl. $\geq$ -11°), the 2.7m Harlan J. Smith telescope at McDonald Observatory was used to observe southern targets below this limit. Observations were made during one observing run from 25-29 July 2003. The Imaging Grism Instrument (IGI) spectrograph was used with a 6000Å Grism, and a 50mm lens. A $2''$ slit was employed for the first 1.5 nights, and a $2.5''$ slit thereafter due to generally poor seeing. The image FWHM fluctuated between $1.5''$ and $2''$ on the best night, but typically held around 2-2.5$''$. The IGI setup covered a smaller wavelength range than the HET/LRS, namely $\lambda\lambda 4250 - 8500$Å. Due to a wide range of conditions and source brightnesses, total exposures ranged from 300 to 3600 seconds.

Standard CCD reductions were performed using IRAF. Spectra were optimally extracted from the 2-d images and calibrated. Telluric corrections were applied to remove atmospheric absorption. Redshifts were estimated by cross-correlation analysis with AGN and galaxy spectral templates, using the IRAF RVSAO package.

As of this publication, we have obtained 26 spectral classifications, 8 with the HET/LRS and 18 with the McDonald 2.7m/IGI. The new redshifts and basic optical properties of these objects are listed in Table 2. Marginal (e.g. single line or low S/N) redshift estimates are denoted by a colon. Spectra taken at McDonald Observatory are plotted in Figure 2. Since

optical observations were initiated before the 8.4 GHz data were reduced, a number of sources in Figure 2 and Table 2 do not appear in Table 1, as their final FoM are below the 'plausible' threshold.

Sources observed at McDonald Observatory were classified based on their spectra, S/N permitting. The observed sources fall into the following 3 categories: BL Lac objects (BLL), flat spectrum radio quasars (FSRQ), and narrow line radio galaxies (NLRG). BL Lac objects are defined here by the following properties (Marcha et al. 1996):
1. H/K break contrast = $(\frac{f^+ - f^-}{f^+}) < 0.4$ where f^+ and f^- are the fluxes redward and blueward of the break.
2. Rest-frame emission line equivalent width < 5Å.
A handful of objects were observed to have narrow emission lines, with kinematic widths <1000 km/s, and equivalent widths larger than the BL Lac threshold. These objects generally exhibit a weak continuum flux, and were consequently classified as NLRGs. The majority of observed sources were FSRQs with broad (v_{kin} > 1000-2000 km/s) emission lines. For the sources with archival redshifts, we examined spectra from the literature whenever possible. When these were unavailable the NED/SIMBAD classifications were adopted as a last resort.

5. Results

All of the 3EG error boxes located in the region -40° < decl. < 0° are listed in Table 1, along with classifications and new counterpart candidates. We recover many of the counterparts identified in the Third EGRET Catalog (Hartman *et al.* 1999) and by Mattox (Mattox *et al.* 2001). Those that did not meet our selection criteria are included for completeness (italics). We also indicate in the classification column sources that are previously discussed pulsar/plerion candidates (p).

The spectral index listed in the table is calculated between 1.4 GHz and 8.4 GHz, where $S_\nu \propto \nu^{-\alpha}$, with the exception of indices listed in parentheses which were calculated between 1.4 GHz and 4.8 GHz. A radio ID flag, RID, was included to indicate the origin of the radio flux: the VLA Calibrator Survey, this campaign, or both.

Sources are divided into high and lower confidence identifications by their FoMs. Lower confidence ('plausible') identifications fall in the range 0.25 <FoM< 1.0, and higher confidence ('likely') source identifications have FoM ≥ 1. In the -40° < decl. < 0° band we have identified 30 likely and 23 plausible counterparts with 8.4 GHz flux measurements (5 nominally 'likely' counterparts lacking 8.4 GHz confirmation deserve follow-up, but as noted above the 28 additional sources classified as 'plausible' based on extrapolated fluxes are

mostly at low b, are very likely Galactic, and are designated 'G' in Table 1). Despite the rather cautious labels, the sources with 8.4 GHz observations are statistically highly significant identifications; simulations based on the Northern survey indicate a success rate of 92% for the likely sources and 82% for the plausible sources. Thus among 'likely' sources with 8.4 GHz measurements (of which 7 are newly identified here) we statistically expect 2 false positives. For the 'plausible' sources (16 of which are new) we expect no more than 4 false identifications.

As in the north, we find evidence in this Southern extension for multiple counterparts for individual 3EG sources, where the fainter radio counterpart(s) would be ignored in the 3EG/Mattox studies. Figure 3 shows two cases, 3EG J1246-0651 and 3EG J1911-2000. 3EG J1246-0651 contains two high-confidence IDs in an elongated error region, with two likelihood maxima corresponding well to the candidate positions. 3EG J1911-2000 also contains two counterparts, one plausible and one high-confidence. Again, the sources line up along the major axis of the error contour. It appears that the centroid of the uncertainty region is shifted slightly from the more likely source toward the fainter radio source, suggesting that a fainter γ-ray contribution biases the TS localization.

5.1. Comparison with the Northern 3EG Sample

A comparison of the populations and luminosity functions of the candidates requires full treatment of the EGRET sensitivities and the radio/X-ray selection biases. We defer this population study to a future communication. However, it is already interesting to make a comparison of the areal densities of various source classes in the combined survey.

The Galactic Aitoff projection in Figure 4 summarizes the current status of the 3EG counterpart identification. In order to compare the different populations, we divide the sky above decl. > -40° into three regions:
– Galactic plane – $|b|$ <10°,
– Galactic bulge (excluding the plane) – $|b|$ >10° and < 30° from $l = b = 0$, and
– high latitude – the remainder.
In the 'high latitude' set, we find 88 blazar IDs and 41 non-blazar IDs, suggesting that 68% or more of the high latitude 3EG detections have radio-bright blazar counterparts. In the bulge region, we find 13 blazar IDs and 15 non-blazar IDs, compared to 4 blazar IDs and 2 non-blazar IDs predicted from the areal density at high latitude. The larger number of sources here, including a factor of 3 more blazars, may be attributed to deeper EGRET exposure (2.5× larger 3EG exposure, averaged over area, in our bulge region relative to the high latitude region.) Even relative to this increase, there is clearly an excess of non-

blazar identifications in the bulge (54% *vs.* 32% at high latitude), which likely represents a new bulge population of $\gamma-$ray sources. Within the plane, we find 12 blazar IDs and 49 non-blazar IDs, compared to 18 blazar IDs and 8 non-blazars predicted from high latitude. The apparent deficit of blazar identifications in the plane may be partly due to decreased EGRET sensitivity in this high background region, although source confusion limitations to counterpart identification may also play a role. The large number of unidentified sources here clearly represents a Galactic population.

Grouping objects by type, we find 17% BL Lacs and 83% FSRQs in the Southern extension, very similar to the 19% BL Lacs and 81% FSRQs in the Northern survey.

We can examine the redshift distributions of the Northern and Southern extension samples, since these should be independent of the initial candidate selection. Before we do so, we include four additional redshifts determined for the Northern sample since the publication of SRM03 (Figure 5, Table 3). Since the BL Lacs and FSRQs form two distinct populations in redshift space, we treat the two samples independently (Figure 6). Similar to the Northern sample, we uncover a handful of $z > 3$ sources in the Southern extension. For the FSRQ sample, we find a good agreement between the north and south, with a Kolmogorov-Smirnov probability of 0.27 that the populations are drawn from the same parent distribution. In the case of BL Lacs, the north and south distributions are still consistent, but with a lower probability – Prob(K-S) = 0.08. However, it should be noted that spectroscopic identification is much more complete in the Northern sample.

6. Individual Object Notes

3EG J0340-0201–In addition to the likely association with J0339-0146 we find a plausible second counterpart in J0339-0133.

3EG J0412-1853–In this large error region, ∼4 degrees in diameter, we find a plausible counterpart, J0409-1948, in addition to the likely ID J0416-1851.

3EG J0530-3626–From the predicted radio flux and 1.4/4.8 GHz spectral index, we believe J0529-3555 to be the most likely counterpart, although this requires confirmation. The previous claim, J0522-3627, with ΔTS = 17.9 lies well to the south of this error map, which is strongly elongated east to west. It does not meet our FoM cut.

3EG J0542-0655–In addition to the previous association, J0541-0541 (plausible), we find an equally likely counterpart based on 1.4/4.8 GHz spectral index and extrapolated flux; again this should be interferometrically confirmed.

3EG J1246-0651–We find two likely associations, J1248-0632 and J1246-0730, in this map. These sources present a strong case for two sources nearly resolved by EGRET. The TS map is shown in Figure 3.

3EG J1500-3509–J1457-3539 and J1505-3432, neither of which were previously identified as γ-ray counterparts, are both likely IDs located within this error map.

3EG J1504-1537–Three plausible sources occupy this error map in addition to the previous ID J1507-1652, which is located well beyond the 99% contour.

3EG J1607-1101–Two plausible and one likely source occupy this map based on extrapolated fluxes and 1.4/4.8 GHz spectral indices. J1605-1139 is claimed as a counterpart by Tornikoski (2002) based on 90 GHz observations, but it does not match our survey criteria.

3EG J1612-2618–Two likely sources are located in this error map, based on 1.4/4.8 GHz spectral indices and extrapolated fluxes. Two plausible sources near the threshold for inclusion are also selected; these are unlikely to pass the compact 8.4 GHz FoM cut.

3EG J1718-3313–The likely counterpart, J1717-3342, which we identify as a BL Lac, is very reddened at its low latitude.

3EG J1746-2851–McLaughlin and Cordes (2003) present evidence that PSR J1747-2958 is the counterpart.

3EG J1800-2338–This γ-ray source has been identified with the pulsar PSR B1758-23.

3EG J1809-2328–This γ-ray source has been identified with a plerion (Roberts, M.S.E. *et al.* 2001; Braje, *et al.* 2002).

3EG J1832-2110–counterparts J1832-2039, plausible, and J1833-2103, likely, share this compact, circular error box.

3EG J1911-2000–J1911-2006, high-confidence, and J1911-1921, plausible, are both associations in this error box. The γ-ray flux of J1911-2006 is likely supplemented by that of J1911-1921. The TS map is shown in Figure 3.

3EG J1937-1529–J1935-1602, plausible, and J1939-1525, likely, both lie in this elongated error box. Our analysis does not support the previously claimed counterpart J1941-1524.

3EG J2006-2321–We find the centrally located J2005-2310, previously claimed as a new low radio flux ID by Wallace (2002), to be a likely counterpart.

3EG J2034-3110–One likely ID, J2030-3039, and one plausible ID, J2039-3157, reside

in this large error box. Neither have been previously associated with the EGRET source. The 95% contour is not closed in this map.

7. Conclusions

From our radio follow-up, our FoM method has selected 23 new IDs, with 8.4 GHz fluxes, between -40° < decl. < 0°. Of these new identifications, seven sources have high confidence 'likely' counterparts and the remainder are plausible. We expect no more than 3 of these new sources are false positives. A few additional identifications are based on 4.85 GHz extrapolations and require 8.4 GHz compact fluxes for confirmation. We also have spectroscopically identified 26 new optical counterparts selected for this sample. Several of these targets fell below our FoM after VLA follow-up - the spectroscopic targets were selected before 8.4 GHz fluxes were available - but are included in Table 2 for completeness. Combined with the Northern sample, for high latitude 3EG error boxes ($|b| > 10°$ and >30° from the galactic center), we find blazar IDs for 88 of 129 sources, or 68%. Our analysis has now been applied to 157 of the 186 3EG detections located above $|b| > 10°$.

Extending the survey into the Galactic bulge, we find a surplus of unidentified 3EG sources. These likely comprise a new set of Galactic γ-ray emitters. Since the areal density of identified blazars in the bulge region is also larger than in the North, it seems that the longer EGRET exposure in this region has let us look lower on the blazar luminosity function, which should be helpful in refining the blazar contribution to the unresolved high latitude γ-ray counts. We defer detailed calculation of the blazar luminosity function and number count predictions for GLAST to a later paper.

The Hobby-Eberly Telescope (HET) is a joint project of the University of Texas at Austin, the Pennsylvania State University, Stanford University, Ludwig-Maximilians-Universität München, and Georg-August-Universität Göttingen. The HET is named in honor of its principal benefactors, William P. Hobby and Robert E. Eberly.

The Marcario Low Resolution Spectrograph is named for Mike Marcario of High Lonesome Optics who fabricated several optics for the instrument but died before its completion. The LRS is a joint project of the Hobby-Eberly Telescope partnership and the Instituto de Astronomia de la Universidad Nacional Autonoma de Mexico.

The National Radio Astronomy Observatory is a facility of the National Science Foundation operated under cooperative agreement by Associated Universities, Inc.

DSE was supported by SLAC under DOE contract DE-AC03-76SF00515 and PFM

acknowledges support from NASA contract NAS5-00147. We thank F. Heatherington for assistance with reduction of the VLA radio data.

REFERENCES

Braje, T.M., Romani, R.W., Roberts, M.S.E., & Kawai, N. 2002, ApJ, 565, L91

Condon, J.J., *et al.* 1998, AJ, 115, 1693

Gregory, P.C., Scott, W.K., Douglas, K. & Condon, J.J. 1996, ApJS, 103, 427

Halpern, J.P., Eracleous, M., Mukherjee, R., & Gotthelf, E.V. 2001, ApJ, 551, 1016

Hartman, R.C., *et al.* 1999, ApJS, 123,79

Hill, G.J., Nicklas, H.E., MacQueen, P.J., Tejada, C., Cobos Duenas, F.J. & Mitsch, W. 1998 Proc. SPIE, 3355, 375

Laurent-Muehleisen, S.A., Kollgaard, R.I., Ciardullo, R., Feigelson, E.D., Brinkmann, W., & Siebert, J. 1998, ApJS, 118,127

Marcha, M.J.M., Browne, I.W.A., Impey, C.D., & Smith, P.S. 1996, MNRAS,281,425

Marcha, M.J., Caccianiga, A., Browne, I.W.A, & Jackson, N. 2001, MNRAS, 326, 1455

Mattox, J.R., *et al.* 1996, ApJ, 461, 396

Mattox, J.R., Hartman, R.C., Reimer, O. 2001, ApJS, 135, 155

McLaughlin, M.A., & Cordes, J.M. 2003, astro-ph0310748

Monet, D.G. *et al.* 2003, AJ, 125, 984

Myers, S.T., Jackson, N.J.,Browne, I.W.A.,Bruyn, A.G., Pearson, T.J., Readhead, A.C.S., Wilkinson, P.N., Biggs, A.D., Blandford, R.D., Fassnacht, C.D., Koopmans, L.V.E., Marlow, D.R., McKean, J.P., Norbury, M.A., Phillips, P.M., Rusin, D., Shepherd, M.C., & Sykes, C.M. 2002, astro-ph/0211073

Perlman, E.S., Padovani, P., Giommi, P., Sambruna, R., Jones, L.R., Tzioumis, A. & Reynolds, J. 1998, AJ, 115, 1253

Landt, H., Padovani, P., Perlman, E.S., Giommi, P., Bignall, H. & Tzioumis, A. 2001, MNRAS, 323, 757

Ramsey, L.W. *et al.* 1998, Proc. SPIE, 3352, 34

Roberts, M.S.E., Romani, R.W., & Kawai, N. 2001, ApJS, 133, 451

Sowards-Emmerd, D., Romani, R. W. & Michelson, P. F. 2003, ApJ, 590, 109

Tornikoski, M. *et al.* 2002, ApJ, 579, 136

Urry, C.M. & Padovani, P. 1995, PASP, 107, 803

Urry, C.M. 1999, *Astpart. Phys.*, 11, 159

Wallace, P.M. Halpern, J.P., Magalhaes, A.M.,& Thompson, D.J. 2002, ApJ, 569, 36

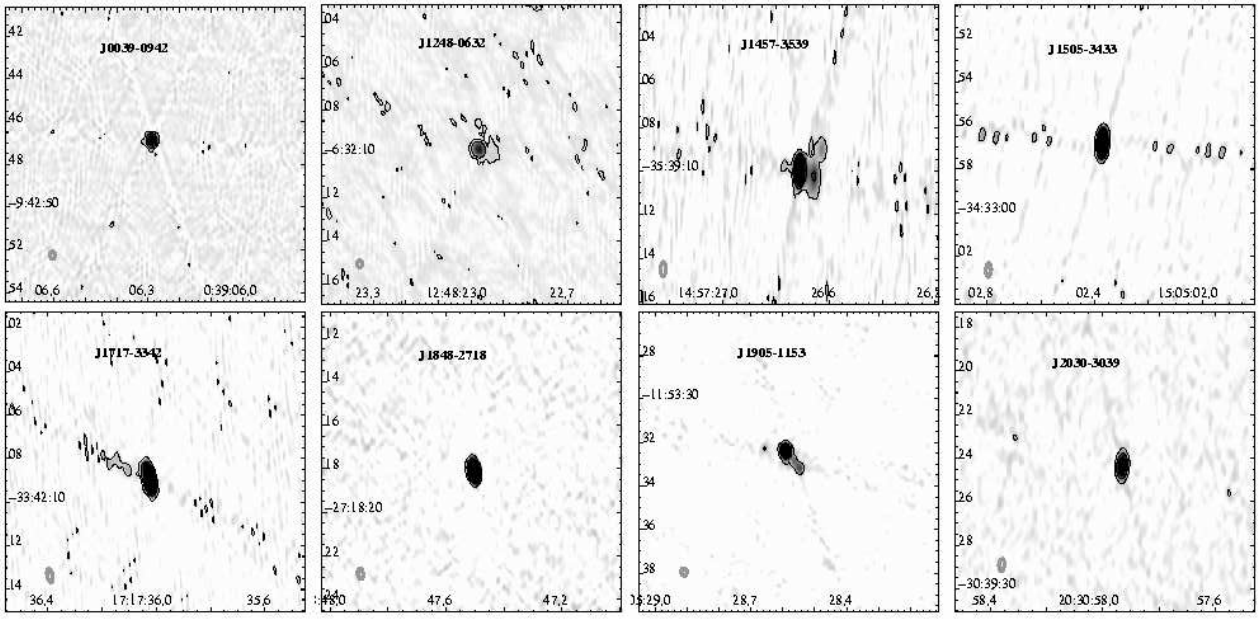

Fig. 1.— Sample VLA 8.4 GHz snapshots of our blazar counterparts. Here the 7 newly identified high confidence 'likely' associations are shown with contours at 1mJy and 10mJy/beam and a logarithmic grey scale to bring out faint noise and source structure. The restoring beam is in grey at the lower left. One lower confidence 'plausible' association with a strong jet (J1905-1153) completes the sample set.

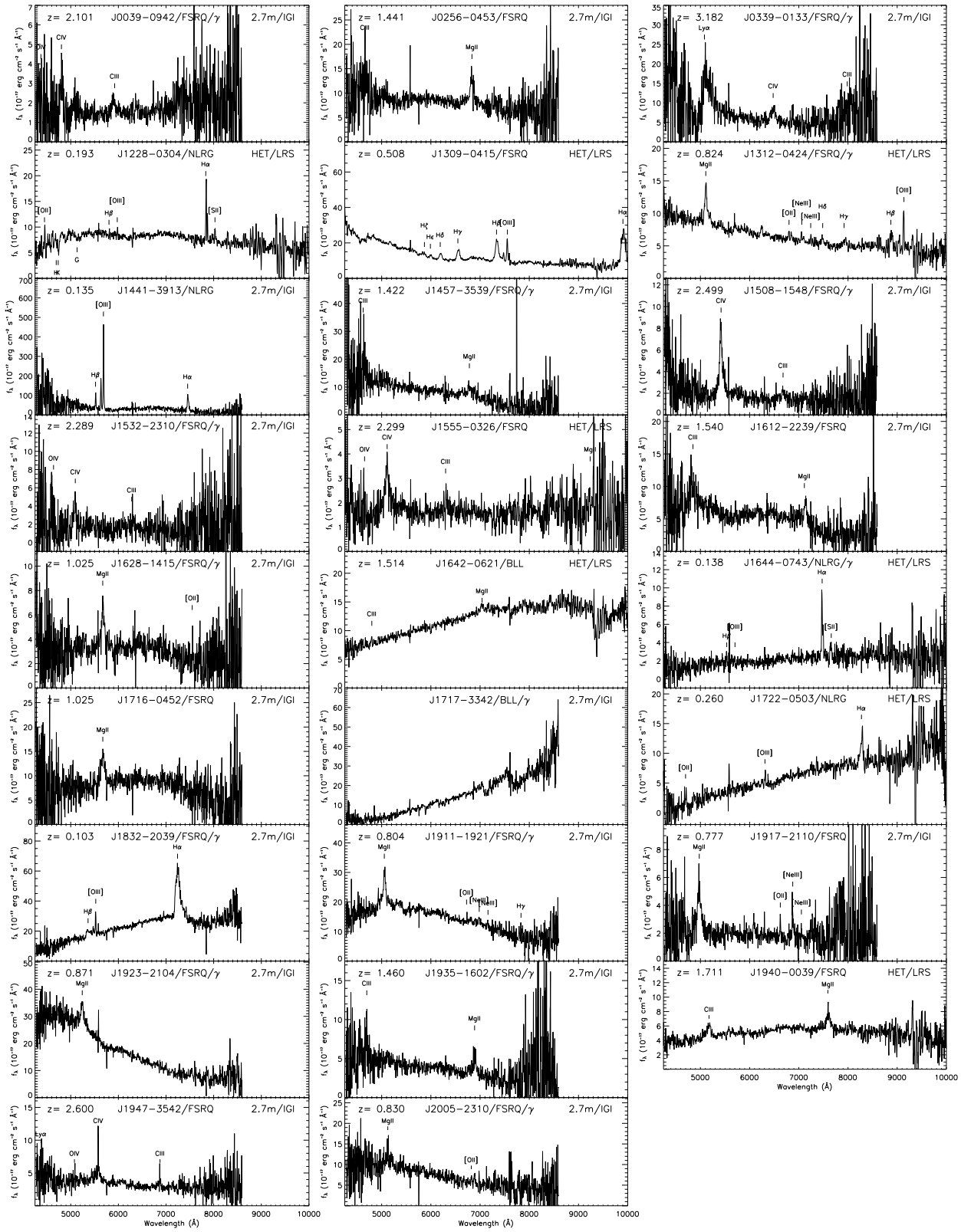

Fig. 2.— HET/LRS and McDonald 2.7m/IGI Spectroscopy

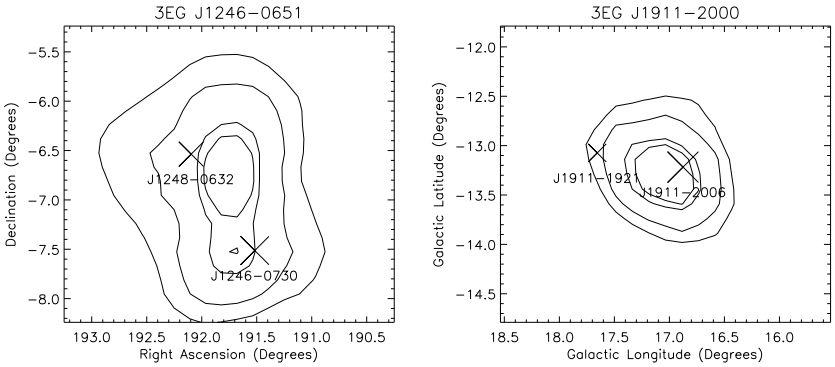

Fig. 3.— 3EG TS maps for two likely composite sources. Contours show 50%, 68%, 95% and 99% uncertainty regions. The blazar counterparts are indicated with crosses.

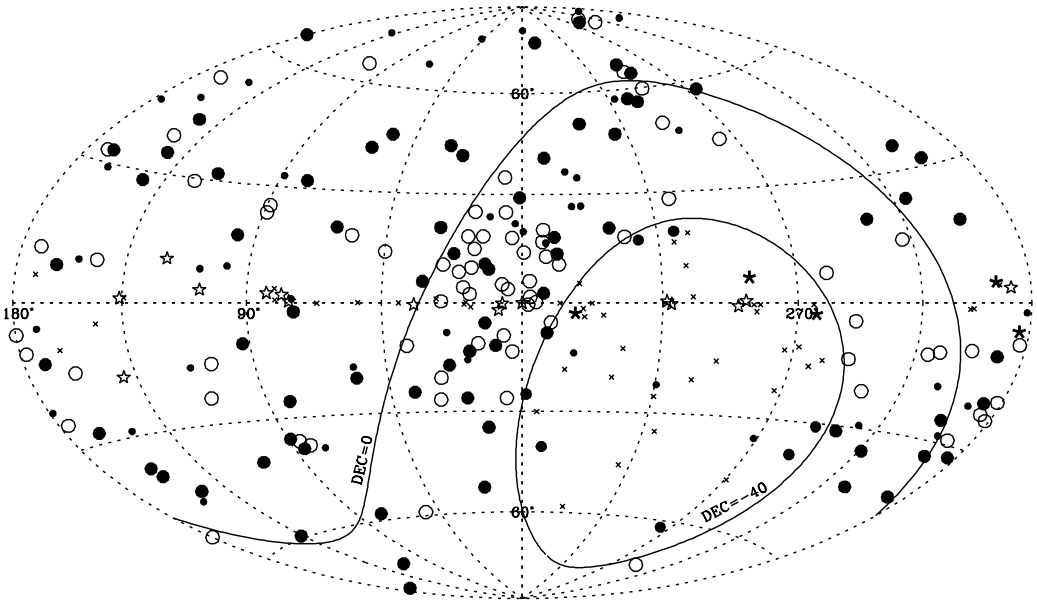

Fig. 4.— Aitoff equal area projection of 3EG sources in Galactic coordinates showing our new classifications; this may be compared with Figure 4 in SRM03. *Large filled circle*, high confidence blazar; *Smaller filled circle*, plausible blazar; *Filled star*, pulsar; *Open star*, pulsar/plerion candidate; *Open circle*, Non-Blazar; *cross*, presently unclassified. Symbols south of decl.=-40° are similar, with AGN drawn from the 3EG A/a classifications.

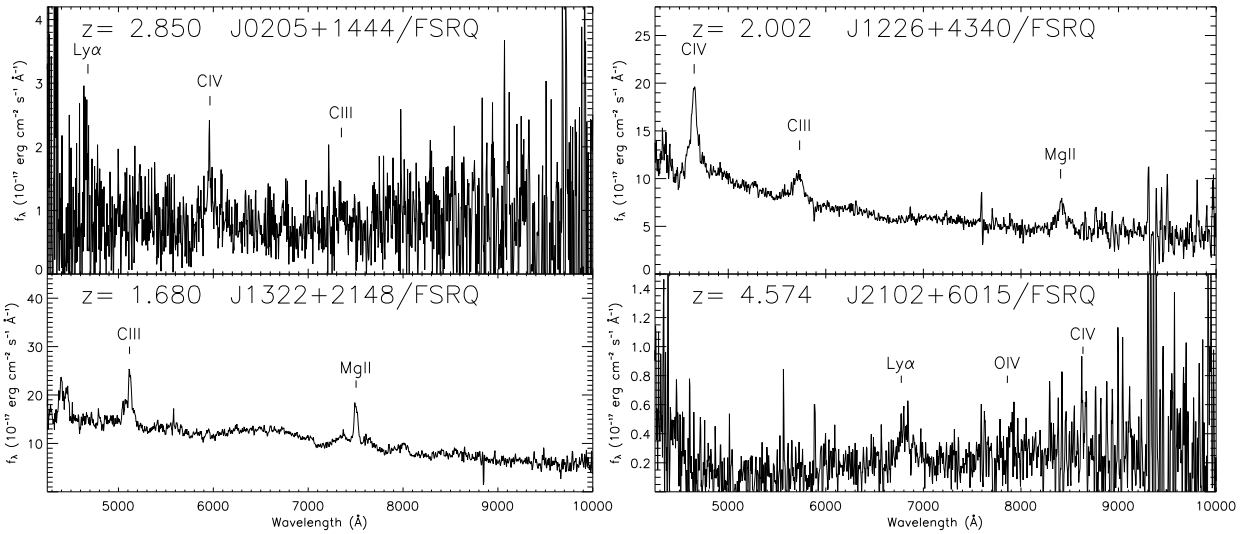

Fig. 5.— HET/LRS spectroscopic observations of northern γ-ray source counterparts obtained since SRM03.

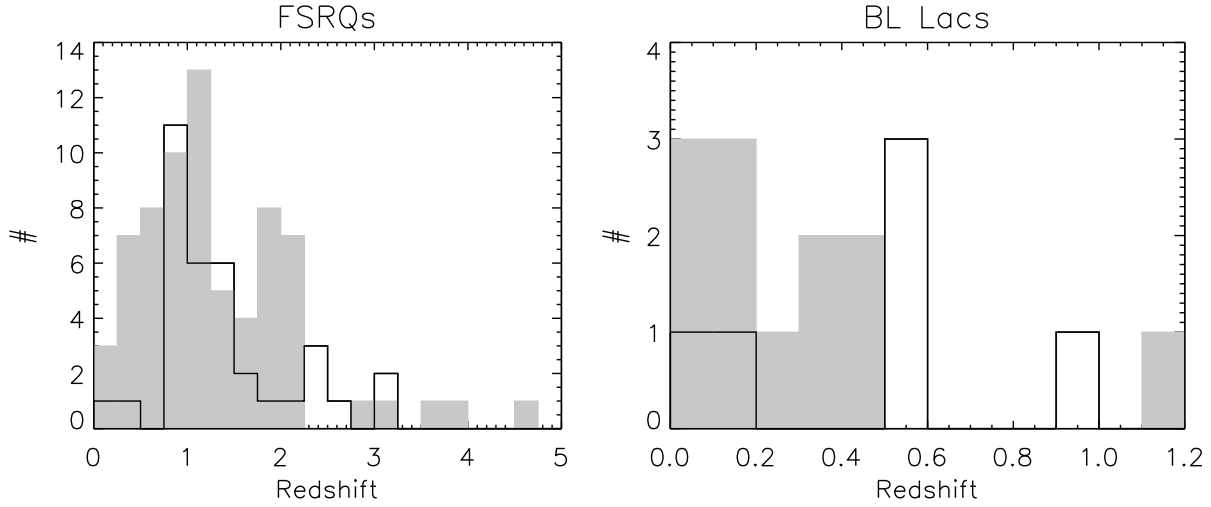

Fig. 6.— Redshift distributions: gray histogram – northern sources, solid line – southern sources

Table 1. 3EG Objects

3EG	γ-type[a]	Identification	$S_{8.4}$(mJy)	α	ΔTS	FoM	z	PID[b]	RID[c]	Mattox[d]	EGRET[e]	Class[f]
J0038-0949	B	**J0039-0942**	187	-0.12	0.46	3.58	2.101	*	1			f
J0130-1758	B	**J0132-1654**	952	-0.08	7.73	1.04	1.020		3		a	f
J0159-3603	N											
J0253-0345	N											
J0340-0201	B	J0339-0133	339	0.28	6.69	0.42	3.182	†*	1			f
		J0339-0146	3010	-0.13	3.49	3.59	0.852		3	+	A	f
J0412-1853	B	J0409-1948	108	0.11	3.06	0.32	1.986	†	1			f
		J0416-1851	780	0.23	1.91	2.30	1.536		3	–	A	f
J0422-0102	B	**J0423-0120**	4250	-0.2	4.81	4.03	0.915		2	+	A	f
J0442-0033	b	J0442-0017	860	0.39	4.56	0.54	0.844		2	+	A	f
J0456-2338	B	**J0457-2324**	1850	-0.0	0.95	7.42	1.003		2	+	A	f
J0500-0159	B	**J0501-0159**	3700	-0.25	0.86	10.60	2.286		2	+	A	f
J0530-3626	B	**J0529-3555**	(289)	(-0.42)	2.29	(4.07)	–	(*)	0			
		J0522-3627	5000	0.63	17.9	0.00	0.061		2		a	b
J0531-2940	b	J0539-2839	760	0.06	9.83	0.32	3.104		2		a	f
J0542-0655	b	J0541-0541	980	-0.06	10.33	0.34	0.839		2		a	f
		J0545-0539	(151)	(0.11)	6.48	(0.34)	–		0			
J0616-0720	N											
J0616-3310	N											
J0622-1139	N	*J0619-1140*	210	0.47	3.76	0.13	–		1	–	A	
J0706-3837	N											
J0747-3412	N											
J0812-0646	N	*J0808-0751*	2600	-0.29	14.19	0.05	1.837		2		a	f
J0852-1216	B	**J0850-1213**	625	-0.37	2.67	5.04	0.57		1	–	A	b
J0903-3531	N											
J1134-1530	N	*J1130-1449*	3060	0.30	18.71	0.01	1.187		2		a	f
J1219-1520	b	J1222-1645	145	0.03	7.73	0.25	–	*	1			
J1230-0247	N	*J1232-0224*	629	0.50	3.25	0.15	1.045		1	–	A	f
J1234-1318	N											
J1246-0651	B	**J1248-0632**	353	0.02	3.21	1.83	0.762	†	1			f
		J1246-0730	630	-0.08	2.09	4.05	1.286		2	–	A	f
J1255-0549	B	**J1256-0547**	15600	-0.2	6.99	3.65	0.538		2	+	A	b
J1310-0517	b	J1312-0424	286	-0.15	7.85	0.67	0.824	*	1			f
J1314-3431	b	J1316-3338	1100	0.07	12.5	0.14	1.210		1		a	f
J1339-1419	B	**J1337-1257**	3850	-0.21	5.75	3.38	0.539		3	+	A	b
J1409-0745	B	**J1408-0752**	630	0.00	3.50	2.19	1.494		2	+	A	f
J1447-3936	N											
J1457-1903	b	J1459-1810	158	-0.24	9.82	0.25	–	*	1			
J1500-3509	B	**J1457-3539**	606	0.04	4.27	1.76	1.422	†*	1			f
		J1505-3432	393	-0.59	4.32	3.37	–	*	1			
J1504-1537	b	J1502-1508	133	-0.18	5.25	0.62	–	*	1			
		J1505-1610	130	-0.24	5.43	0.61	–	*	1			
		J1508-1548	307	-0.03	8.50	0.41	2.499	*	1			f
		J1507-1652	2400.	0.05	13.97	0.03	0.876		2		a	f
J1512-0849	B	**J1512-0905**	2150	0.12	1.79	4.31	0.360		2	+	A	f
J1517-2538	b	J1517-2422	1930	0.02	9.18	0.44	0.049		3	–	a	b
J1527-2358	b	J1532-2310	158	-0.09	5.82	0.64	2.289	*	1			f
J1600-0351	N											
J1607-1101	B	J1603-1007	(146)	(0.08)	6.75	(0.32)	–		0			
		J1605-1012	(127)	(-0.27)	4.15	(0.76)	–		0			
		J1612-1133	(169)	(-0.58)	4.91	(1.52)	–	(*)	0			
		J1605-1139[g]										
J1612-2618	B	J1607-2656	(119)	(0.29)	2.55	(0.30)	–		0			
		J1611-2612	(113)	(-0.17)	0.32	(1.54)	–	(*)	0			
		J1613-2750	(210)	(0.05)	8.54	(0.26)	–		0			
		J1617-2537	(153)	(-0.15)	3.06	(1.22)	–	(*)	0			
J1616-2221	N											
J1625-2955	B	**J1626-2951**	2250	-0.00	4.06	2.58	0.815		2	+	A	f
J1626-2519	b	J1625-2527	1100	0.45	0.65	0.99	0.786		2	+	A	f
J1627-2419	N											
J1631-1018	N											
J1633-3216	N											
J1634-1434	b	J1628-1415	275	0.14	6.85	0.54	1.025	†*	1			f
J1635-1751	b	J1629-1720	(245)	(-0.56)	9.70	(0.39)	–		0			
J1638-2749	N											
J1646-0704	b	J1644-0743	129	-0.08	4.73	0.55	0.139	*	1			r
J1649-1611	N											

Table 1—Continued

3EG	γ-type[a]	Identification	$S_{8.4}$(mJy)	α	ΔTS	FoM	z	PID[b]	RID[c]	Mattox[d]	EGRET[e]	Class[f]
J1652-0223	N											
J1653-2133	N											
J1709-0828	N											
J1714-3857	G	J1711-3908	(25100.)	(-1.98)	9.49	(0.71)	–		0			(G)
		J1712-3840	(468)	(-0.98)	4.87	(3.34)	–		0			(G)
		J1713-3900	(4340)	(-1.06)	0.00	(19.36)	–		0			(G)
		J1714-3810	(10100)	(-0.84)	9.06	(0.94)	–		0			(G)
		J1714-3937	(165)	(-1.31)	9.43	(0.28)	–		0			(G)
		J1714-3925	(203)	(-1.76)	6.56	(1.31)	–		0			(G)
		J1715-3913	(4300)	(-1.34)	1.81	(11.08)	–		0			(G)
J1717-2737	N											
J1718-3313	B	**J1717-3342**	685	-0.06	2.87	3.18	–	*	1			b
J1719-0430	N											
J1726-0807	N											
J1733-1313	B	**J1733-1304**	5110	0.07	3.90	2.86	0.902		3	+	A	b
J1734-3232	N											
J1735-1500	B	**J1738-1503**	(247)	(0.15)	3.28	(1.06)	–	(*)	0			
J1736-2908	N											
J1741-2050	N											
J1741-2312	N											
J1744-0310	B	**J1743-0350**	6240	-0.84	3.99	5.98	1.054		3	+	A	f
J1744-3011	N											
J1744-3934	N											
J1746-1001	N											
J1746-2851	N	PSR J1747-2958										p
J1757-0711	N											
J1800-0146	N											
J1800-2338	N	PSR B1758-23										p
J1800-3955	B	**J1802-3940**	1700	0.14	2.59	2.74	–		1	–	A	
J1809-2328	N	RRK										p
J1810-1032	N											
J1812-1316	N											
J1823-1314	G	J1822-1251	(753)	(-1.39)	12.48	(0.32)	–		0			(G)
		J1824-1251	(928)	(-1.01)	11.61	(0.46)	–		0			(G)
		J1825-1315	(15300)	(-1.33)	8.48	(1.36)	–		0			(G)
J1824-1514	G	J1819-1501	(2260)	(-0.80)	13.25	(0.27)	–		0			(G)
		J1819-1530	(982)	(-1.28)	10.31	(0.66)	–		0			(G)
		J1821-1449	(6150)	(-1.98)	10.87	(0.66)	–		0			(G)
		J1822-1550	(316)	(-1.88)	10.00	(0.45)	–		0			(G)
		J1822-1602	(342)	(-1.98)	10.43	(0.43)	–		0			(G)
		J1825-1449	(2550)	(-1.05)	4.00	(5.62)	–		0			(G)
		J1826-1600	(269)	(-0.99)	10.00	(0.41)	–		0			(G)
J1826-1302	G	J1824-1251	(918)	(-1.01)	6.32	(3.00)	–		0			(G)
		J1825-1315	(15100)	(-1.33)	3.82	(5.24)	–		0			(G)
		J1826-1338	(245)	(-1.26)	6.60	(1.53)	–		0			(G)
J1832-2110	B	J1832-2039	1070	0.03	8.18	0.70	0.103	*	1			f
		J1833-2103	6750.	0.25	4.31	1.29	2.510		2	+	A	f
J1834-2803	N											
J1837-0423	G	J1837-0508	(276)	(-1.92)	10.74	(0.35)	–		0			(G)
		J1839-0419	(1890)	(-1.60)	5.43	(4.19)	–		0			PN
J1837-0606	N											
J1847-3219	N											
J1850-2652	B	**J1848-2718**	417	-1.26	2.38	5.85	–	*	1			
J1858-2137	N											
J1904-1124	b	J1905-1153	154	0.26	3.09	0.48	–	*	1			
J1911-2000	B	**J1911-2006**	2190	0.11	0.12	6.75	1.119		3	+	A	f
		J1911-1921	182	0.06	6.84	0.45	0.804	*	1			f
J1921-2015	b	J1923-2104	2190	0.19	8.94	0.32	0.871		1	–	a	f
J1937-1529	B	J1935-1602	286	0.04	6.68	0.73	1.460	*	1			f
		J1939-1525	670	-0.0	1.69	4.75	1.657		2	–	A	f
		J1941-1524					0.452			–		r
J1940-0121	N											
J1949-3456	N											
J1955-1414	N											
J2006-2321	B	**J2005-2310**[h]	230	0.14	0.36	2.70	0.830		1	–		f
J2020-1545	N											
J2025-0744	B	**J2025-0735**	727	0.33	0.89	2.20	1.388		1	–	A	f

Table 1—Continued

3EG	γ-type[a]	Identification	$S_{8.4}$(mJy)	α	ΔTS	FoM	z	PID[b]	RID[c]	Mattox[d]	EGRET[e]	Class[f]
J2034-3110	B	**J2030-3039**	229	-0.05	5.45	1.00	–	*	1			
		J2039-3157	231	0.06	6.24	0.67	–	*	1			
J2158-3023	B	**J2158-3013**	204	0.44	0.36	1.21	0.117		1	–	A	b
J2251-1341	N											
J2321-0328	B	**J2323-0317**	918	-0.00	1.97	5.12	1.411		3	–	A	f

Note. — Our high confidence associations are listed in boldface and our lower confidence associations in plain text. Previously claimed AGN associations not supported by our analysis are given in italics. () entries are PREDICTED values extrapolating from 1.4/4.8 GHz to 8.4 GHz.

[a]$\gamma-$ray source classification: N = non-blazar, b = plausible blazar ID, B = high confidence blazar ID, G = likely galactic

[b]New associations and/or redshifts: asterisk indicates new spectral identification, dagger indicates archival classification.

[c]Radio data origin: 0 = not observed, 1 = this VLA campaign, 2 = VLA Calibrator survey, 3 = both, fluxes from this VLA campaign are listed.

[d]Mattox *et al.* 2001 selected blazars: + = high probability, - = plausible

[e]Third EGRET Catalog blazars: A = high confidence, a = lower confidence

[f]Classification: b = BL Lac , f = FSRQ, r = NLRG, p = pulsar/plerion, G = likely galactic, PN = Planetary Nebula

[g]Tornikoski *et al.* 2002

[h]Wallace *et al.* 2002

Table 2. HET/LRS and McDonald 2.7m/IGI Spectroscopy

Name	FoM	R.A. (J2000)	Dec. (J2000)	R2[a]	B2[a]	z	Type[b]
J0039-0942	3.58	00 39 06.28	-09 42 47.5	...	20.6	2.1015	f
J0256-0453	0.02	02 56 50.35	-04 53 43.7	18.3	19.9	1.4410	f
J0339-0133	0.42	03 39 00.94	-01 33 18.1			3.1826	f
J1228-0304	0.20	12 28 36.91	-03 04 39.3	19.7	20.2	0.1930	r
J1309-0415	0.00	13 09 17.81	-04 15 15.2	18.8	19.0	0.5089	f
J1312-0424	0.67	13 12 50.92	-04 24 50.7	19.3	18.7	0.8249	f
J1441-3913	0.00	14 41 15.13	-39 13 48.4	14.9	15.2	0.1356	r
J1457-3539	1.76	14 57 26.76	-35 39 09.2	18.9	17.8	1.4222:	f
J1508-1548	0.41	15 08 35.69	-15 48 31.6	19.2	20.2	2.4990	f
J1532-2310	0.64	15 32 31.53	-23 10 32.2	19.7	21.4	2.2896	f
J1555-0326	0.16	15 55 30.80	-03 26 49.4	19.7	20.7	2.2996	f
J1612-2239	0.02	16 12 28.48	-22 39 46.8	19.5	19.6	1.5404	f
J1628-1415	0.54	16 28 46.71	-14 15 41.9	...	20.4	1.0255	f
J1642-0621	0.00	16 42 02.22	-06 21 23.6	19.2	20.9	1.5143:	b
J1644-0743	0.55	16 44 52.03	-07 43 43.4	...	...	0.1389	r
J1717-3342	3.18	17 17 36.01	-33 42 08.1	...	...	...	b
J1716-0452	0.12	17 16 26.57	-04 52 12.5	18.7	20.6	1.0258	f
J1722-0503	0.08	17 22 03.61	-05 03 25.8	18.5	...	0.2606	r
J1832-2039	0.70	18 32 11.10	-20 39 47.9	...	20.2	0.1033	f
J1911-1921	0.45	19 11 56.50	-19 21 52.0	18.3	18.5	0.8046	f
J1917-2110	0.13	19 17 08.66	-21 10 31.2	...	21.5	0.7775	f
J1923-2104	0.32	19 23 32.20	-21 04 33.8	...	...	0.8719	f
J1935-1602	0.73	19 35 35.79	-16 02 32.3	19.3	20.1	1.4602	f
J1940-0039	0.01	19 40 09.00	-00 39 01.3	17.0	18.1	1.7110	f
J1947-3542	0.00	19 47 22.65	-35 42 04.2	19.2	19.9	2.600:	f
J2005-2310	2.70	20 05 56.61	-23 10 28.1	18.8	19.6	0.8301:	f

[a]R2 and B2 are USNO B1.0 optical magnitudes (Monet *et al.* 2003).

[b]Classification: b = BL Lac , f = FSRQ, r = NLRG

Table 3. HET Spectroscopy: Northern Followup

Name	FoM	R.A. (J2000)	Dec. (J2000)	R2[a]	B2[a]	z	Type[b]
J0205+1444	2.58	02 05 13.12	+14 44 32.4	...	...	2.8504	f
J1226+4340	0.95	12 26 57.91	+43 40 58.4	19.2	19.3	2.0023	f
J1322+2148	0.29	13 22 11.40	+21 48 12.3	19.4	19.3	1.6803	f
J2102+6015	0.41	21 02 40.22	+60 15 09.8	...	...	4.5749:	f

[a]R2 and B2 are USNO B1.0 optical magnitudes (Monet *et al.* 2003).

[b]Classification: f = FSRQ

Table 4. VLA 'A' Array 8.4 GHz Observations

Name	Flux [mJy]	R. A. (J2000)	Decl. (J2000)	Class
J0039-0942	187 ± 6	00 39 06.291	-09 42 46.88	
J0128-1722	117 ± 4	01 28 01.393	-17 22 24.25	Jet?
J0132-1654	952 ± 29	01 32 43.487	-16 54 48.52	
J0239-0234	595 ± 18	02 39 45.472	-02 34 40.91	
J0256-0453	87.4 ± 2.6	02 56 50.420	-04 53 43.50	
J0339-0133	339 ± 10	03 39 00.985	-01 33 17.60	
J0339-0146	3010 ± 90	03 39 30.937	-01 46 35.80	
J0405-1906	31.0 ± 0.9	04 05 49.678	-19 06 57.27	
J0409-1948	108 ± 3	04 09 40.549	-19 48 01.78	
J0416-1851	779 ± 23	04 16 36.544	-18 51 08.34	Jet?
J0522-2955	47.3 ± 1.6	05 23 00.131	-29 55 17.36	
J0527-3708	0.			
J0531-3533	122 ± 4	05 31 30.419	-35 33 32.65	
J0615-3355	121 ± 4	06 15 12.689	-33 55 53.07	
J0619-1140	210 ± 6	06 19 04.103	-11 40 54.89	
J0621-1259	0.			PN
J0625-1133	183 ± 6	06 25 49.339	-11 33 24.37	Jet?
J0703-3746	0.			
J0710-3813	18.9 ± 1.4	07 10 47.043	-38 13 45.72	
J0713-3812	23.8 ± 0.9	07 13 01.858	-38 12 28.22	
J0747-3310	131 ± 9	07 47 19.693	-33 10 47.03	
J0754-3448	0.			
J0848-1159	42.5 ± 1.3	08 48 47.491	-11 59 53.68	
J0850-1213	625 ± 19	08 50 09.634	-12 13 35.39	Jet?
J0856-1105	357 ± 11	08 56 41.805	-11 05 14.42	Jet?
J1222-1645	145 ± 4	12 22 16.097	-16 45 54.89	
J1223-1544	61.3 ± 1.8	12 23 12.272	-15 44 06.63	Jet?
J1228-0304	128 ± 4	12 28 36.916	-03 04 39.32	
J1231-1236	80.6 ± 2.4	12 31 50.265	-12 36 37.04	
J1232-0224	629 ± 19	12 32 00.014	-02 24 04.80	Jet
J1246-0730	682 ± 20	12 46 04.232	-07 30 46.57	
J1248-0632	353 ± 11	12 48 22.975	-06 32 09.80	Jet?
J1308-0500	0.			
J1309-0415	84.7 ± 2.5	13 09 17.831	-04 15 16.20	
J1312-0424	286 ± 9	13 12 50.900	-04 24 49.88	
J1316-3338	1100 ± 30	13 16 07.985	-33 38 59.17	Jet?
J1316-3429	0.			
J1332-1402	154 ± 5	13 32 30.929	-14 02 13.16	Jet?
J1332-1256	99.4 ± 3.0	13 32 39.251	-12 56 15.34	
J1337-1257	3850 ± 120	13 37 39.782	-12 57 24.69	
J1441-3913	68.9 ± 2.1	14 41 15.088	-39 13 48.03	
J1443-3908	36.7 ± 1.1	14 43 57.197	-39 08 39.73	
J1457-3539	606 ± 18	14 57 26.711	-35 39 09.98	Jet
J1459-1810	158 ± 5	14 59 28.763	-18 10 45.19	
J1502-1508	133 ± 4	15 02 25.017	-15 08 52.50	
J1505-1610	130 ± 4	15 05 22.950	-16 10 40.60	

Table 4—Continued

Name	Flux [mJy]	R. A. (J2000)	Decl. (J2000)	Class
J1505-3432	393 ± 12	15 05 02.371	-34 32 56.83	
J1507-1652	2090 ± 60	15 07 04.786	-16 52 30.26	Jet?
J1508-1548	307 ± 9	15 08 35.700	-15 48 31.51	
J1513-2558	72.7 ± 2.2	15 13 53.174	-25 58 30.16	Jet
J1517-2618	92.2 ± 2.8	15 17 26.621	-26 18 18.99	
J1517-2422	1930 ± 60	15 17 41.813	-24 22 19.47	Jet
J1530-2410	55.6 ± 1.7	15 30 17.018	-24 10 46.41	
J1532-2310	158 ± 5	15 32 31.529	-23 10 32.43	Jet?
J1555-0326	232 ± 7	15 55 30.748	-03 26 49.51	Jet?
J1612-2239	107 ± 3	16 12 28.444	-22 39 46.68	
J1626-2951	1140 ± 30	16 26 06.020	-29 51 26.97	
J1627-2426	71.2 ± 2.1	16 27 00.008	-24 26 40.44	
J1627-0939	2.95 ± 0.15	16 27 45.453	-09 39 45.58	
J1628-1415	275 ± 8	16 28 46.618	-14 15 41.82	
J1632-1052	140 ± 4	16 32 50.108	-10 52 31.94	
J1634-1440	0.			
J1639-0715	14.4 ± 0.4	16 39 21.996	-07 15 33.12	
J1644-0750	1.12 ± 0.12	16 44 00.768	-07 50 00.54	
J1644-0743	129 ± 4	16 44 52.058	-07 43 43.10	
J1653-0150	68.3 ± 2.1	16 53 57.800	-01 49 59.32	
J1716-0452	436 ± 13	17 16 26.487	-04 52 11.94	
J1717-3342	685 ± 21	17 17 36.028	-33 42 08.91	Jet
J1719-2720	27.0 ± 0.8	17 19 59.708	-27 20 42.60	
J1721-2711	0.			PN
J1722-0503	310 ± 9	17 22 03.539	-05 03 25.00	Jet
J1729-0735	103 ± 3	17 29 34.946	-07 35 32.38	
J1733-1304	5110 ± 150	17 33 02.705	-13 04 49.54	Jet?
J1734-3314	0.			
J1740-1515	55.5 ± 1.7	17 40 03.344	-15 15 52.89	
J1743-0350	6240 ± 190	17 43 58.856	-03 50 04.61	
J1800-3849	46.1 ± 1.4	18 00 11.821	-38 49 52.50	Extended
J1802-3940	1700 ± 50	18 02 42.677	-39 40 07.90	Jet?
J1802-0207	1.36 ± 0.14	18 02 49.678	-02 07 49.15	
J1832-2039	1070 ± 30	18 32 11.047	-20 39 48.20	Jet
J1837-0629	0.			SNR025.5+00.2
J1837-0616	0.			
J1848-2718	417 ± 13	18 48 47.504	-27 18 18.09	
J1850-2740	90.0 ± 2.7	18 50 13.979	-27 40 20.92	
J1905-1153	154 ± 5	19 05 28.591	-11 53 32.38	Jet
J1911-2006	2190 ± 70	19 11 09.652	-20 06 55.10	Jet?
J1911-1921	182 ± 5	19 11 56.517	-19 21 50.97	Jet
J1917-2110	195 ± 6	19 17 08.642	-21 10 30.78	
J1923-2104	2200 ± 70	19 23 32.189	-21 04 33.33	
J1935-1602	286 ± 9	19 35 35.795	-16 02 32.38	
J1940-0039	89.1 ± 2.7	19 40 09.000	-00 39 02.01	Jet
J1947-3542	33.5 ± 1.0	19 47 22.624	-35 42 03.69	

Table 4—Continued

Name	Flux [mJy]	R. A. (J2000)	Decl. (J2000)	Class
J1952-3412	116 ± 3	19 52 00.109	-34 12 26.45	Jet
J2005-2310	230 ± 7	20 05 56.594	-23 10 27.01	
J2025-0735	727 ± 22	20 25 40.659	-07 35 52.70	Jet
J2030-3039	229 ± 7	20 30 57.931	-30 39 24.36	
J2039-3157	231 ± 7	20 39 08.653	-31 57 03.90	
J2158-3013	204 ± 6	21 58 52.064	-30 13 32.10	Jet
J2318-0352	81.2 ± 2.4	23 18 15.623	-03 52 14.85	Jet?
J2323-0150	233 ± 7	23 23 04.629	-01 50 48.10	
J2323-0317	918 ± 28	23 23 31.953	-03 17 05.02	Jet?
J2326-0202	226 ± 7	23 26 53.776	-02 02 13.76	Jet

Note. — Peak 8.4 GHz flux densities and positions are based on 2-d gaussian (IMFIT) fits to the bright core. Estimated 3% calibration errors have been added in quadrature to the fit errors. The 'Class' column describes the source morphology: Jet = distinct jet, Jet? = possible jet. A few known non-blazar sources are also indicated.